Aerodynamic interference and vortex-induced vibrations on parallel bridges: The Ewijk bridge during different stages of refurbishment

T. Argentini *, D. Rocchi, A. Zasso

Politecnico di Milano, Department of Mechanical Engineering, via La Masa 1, 20156 Milano, Italy

Received 21 February 2015 Received
in revised form 13 July 2015
Accepted 29 July 2015

1. Introduction

When bridges are located in parallel configuration their wind induced response becomes in general more complex than considering the single stand-alone bridge, due to the aerodynamic interference between the two decks. Several researches have been conducted in the last few years on this topic, since the need for increasing the traffic capacity of existing motorways is becoming quite common, and often the solution consists in doubling an existing bridge crossing, or directly building a twin deck bridge. Some examples of relevant parallel bridges whose aerodynamics has been investigated are the Jindo bridge in Korea (Seo et al., 2013; Kim et al., 2013); the Meiko-Nishi, the Onomichi, and the Kansai Airport bridges in Japan (Suzuki et al., 1999; Okubo and Enami, 1972; Honda et al., 1990); the Haihe, the Pingsheng and the Hongdao bridges in China (Meng et al., 2011; Liu et al., 2009); the Fred Hartman and the New Tacoma bridges in the USA (Svensson and Lovett, 1990; Irwin et al., 2005); and the J.P. Duarte bridge in St. Domingo (Larsen et al., 2000). An overall picture of some of these bridges is shown in Fig. 1.

The presence of a new deck parallel to the existing one can affect significantly the aerodynamics of both decks, and it is a good design practice to assess possible problems and countermeasures relying on wind tunnel tests on sectional aeroelastic models.

The main issues on parallel bridges that need to be investigated are

1. interference effects on the steady aerodynamic coefficients;
2. vortex-induced vibrations (VIV) of the bridges and wake-excitation effects on the downstream bridge;
3. interference effects on the aeroelastic stability (flutter or galloping).

This paper presents the results of the investigations on the aerodynamic interference effects of the Ewijk bridge, achieved using sectional deck models in a 1:50 length scale, in the wind tunnel of Politecnico di Milano.

2. The Ewijk bridge

The Ewijk bridge crosses the river Waal, which is the main branch of the Rhine in the Netherlands, and it is a vital transportation route between the Port of Rotterdam and mainland Europe. The bridge opened to traffic in 1976, and the 1055 m-long structure has ten spans, with a 480 m-long cable-stayed section over the river. This part of the bridge has a main span of 270 m with two side spans of 105 m. The deck is a steel trapezoidal box girder with orthotropic plates on the top and bottom flanges. The box

* Corresponding author.
E-mail address: tommaso.argentini@polimi.it (T. Argentini).

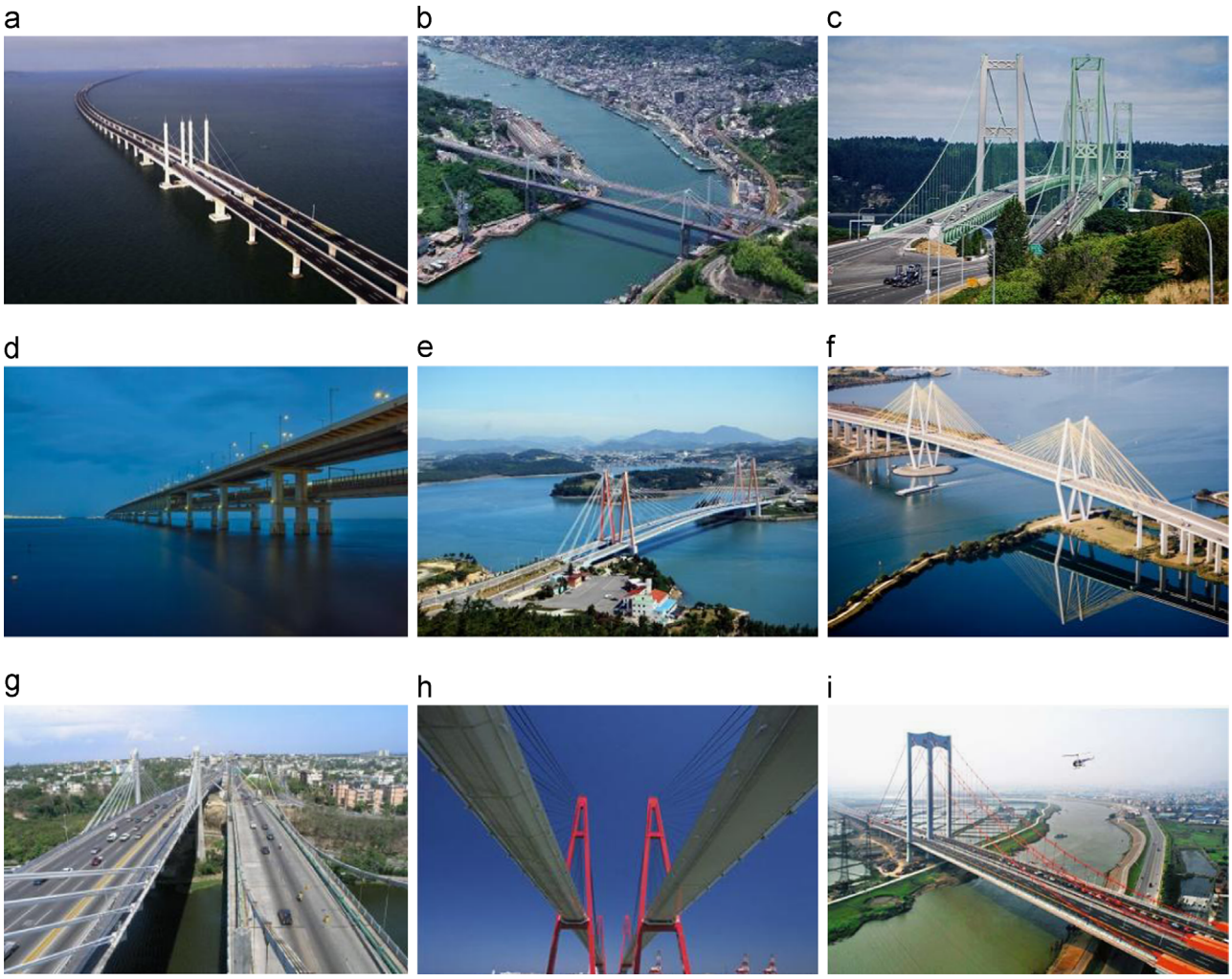

a) Hongdao bridge (China)
b) Onomichi bridge (Japan)
c) New Tacoma Narrows bridge (USA)
d) Kansai Airport Access bridge (Japan)
e) Jindo bridge (Korea)
f) Fred Hartman bridge (USA)
g) J. P. Duarte bridge (S. Domingo)
h) Meiko Nishi bridge (Japan)
i) Pingsheng bridge (China)

Fig. 1. Pictures of some relevant parallel bridges around the world.

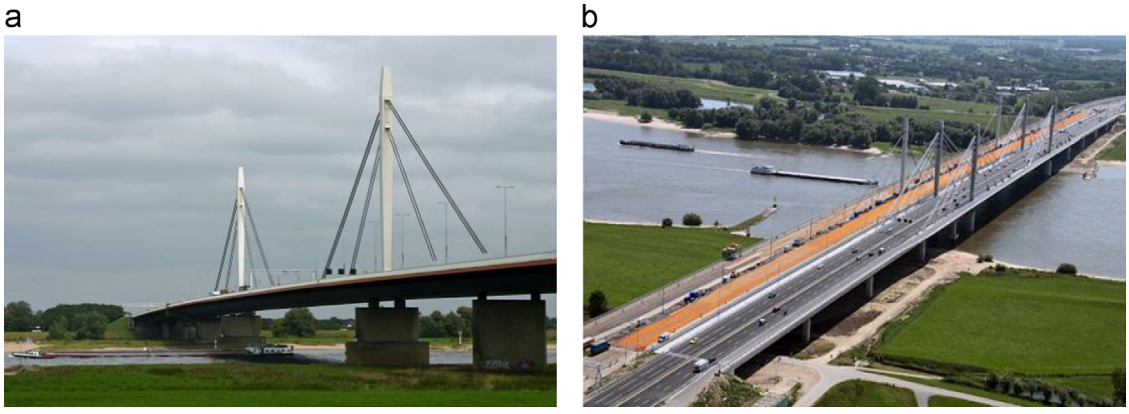

Fig. 2. The Ewijk Bridge. (a) The original stand-alone configuration. (b) The new configuration with the existing deck (in refurbishment) and the new deck.

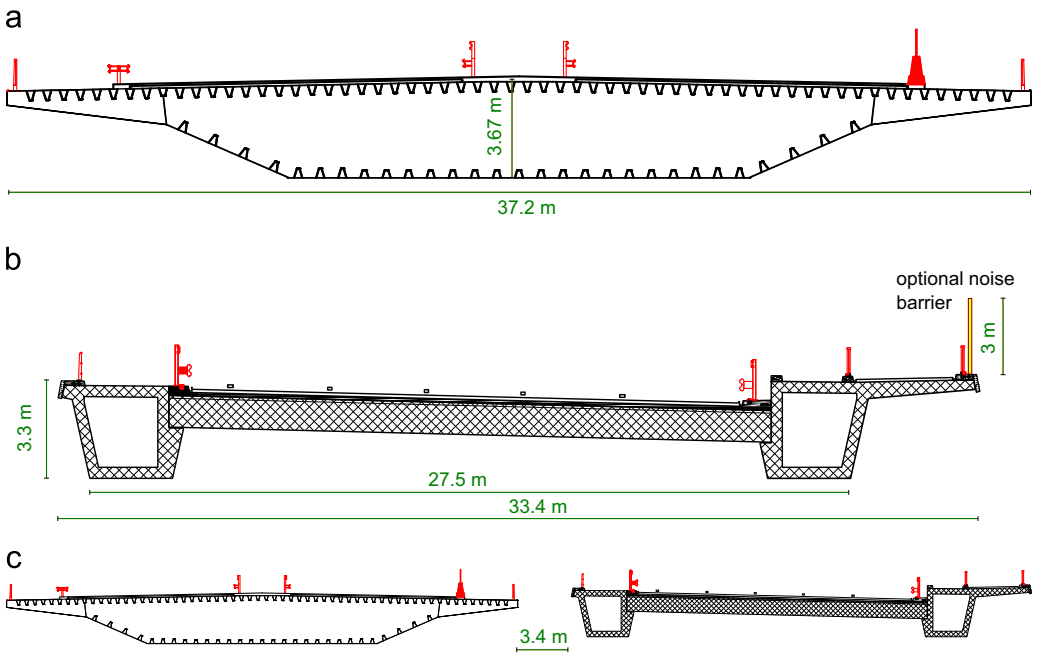

Fig. 3. Existing and new deck sections. Barriers are sketched in red. (For interpretation of the references to color in this figure caption, the reader is referred to the web version of this paper.)

Table 1
Configurations during the refurbishment stages.

Configuration	Variation of height of existing deck (m)	Barriers on existing bridge	Upwind deck
2 - Inner cables removed	+1.2	Removed	New
3 - Outer cables removed	0	Removed	New
4 - In-service	0	Reinstalled	New
5 - In-service + noise barrier	0	Reinstalled + noise barrier on the new bridge	New
6 - In-service	0	Reinstalled	Existing

Table 2
Inertial properties and eigenfrequency values for the two bridges during the refurbishment (full scale).

Bridge	Configuration	Mass per unit length (*ton*/*m*)	Torsional inertia per unit length (*ton m*)	f_v (*Hz*)	f_t (*Hz*)
New bridge	All	75.5	7600	0.38	0.67
Existing bridge	2 and 3	10.3	971	0.49	1.19
	4, 5, and 6	23.2	2239	0.36	0.71

girder is continuous over the ten spans and it is supported by cable stays in the span over the river crossing and in the adjacent spans.

This bridge was selected for renovation due to problems with fatigue cracking in the stay cables (Maljaars and Vrouwenvelder, 2014). To this end, a second bridge was built, next to the existing structure, in order to divert all the traffic off the existing crossing to enable the repairs without loss of traffic capacity (see Fig. 2). After the refurbishment, the new bridge allowed to increase the traffic capacity of the motorway.

The new structure is a cable-stayed bridge, with an asymmetric concrete deck made of two external trapezoidal hollow girders connected by transverse precast beams, evenly spaced along the bridge. Fig. 3 shows a sketch of the two decks with their main elements and dimensions.

During the refurbishment, the existing deck profile, its stiffness and mass are subjected to changes that affect its aerodynamics, structural frequencies, and relative height between new and existing decks (up to 1.2 m). The change of deck shape and mass is due to the presence or not of parapets, asphalt, and traffic barriers on the existing deck, and an optional noise barrier on the new bridge. Tables 1 and 2 summarize some relevant configurations and the corresponding bridge properties, during the refurbishment and at in-service configurations.

The existing deck, in stand-alone configuration, did not suffer of any aerodynamic problems up to the design wind velocity of 30 m/s. The target of the wind tunnel experimental campaign was therefore to assess the interference of the new bridge on the existing one, in terms of effects on static aerodynamic coefficients for bearings verification, effects on aeroelastic stability, and effects on vortex-induced vibrations.

3. Wind tunnels tests

3.1. Experimental setup

The aerodynamic behavior of the two parallel decks was investigated in the boundary layer wind tunnel of Politecnico di Milano (with a test section 14 m wide and 4 m high, and a max wind velocity of 15 m/s). In order to study the interference effect, one rigid sectional model was built for each deck, with a geometrical scale $\lambda_L = 1{:}\ 50$, and with a length ratio of 1:4. A large length scale was chosen to accurately model the details of the traffic barriers and of the parapets (see Fig. 4a and c), that were modeled with an equivalent porosity and a simplified geometry. The edges of the decks were made sharp in order to impose separation points and limit Reynolds effects (at the largest wind speed, Reynolds number was $Re = UD/\nu = 10{\cdot}3.67/1.5{\cdot}10^{-5} = 5.5{\cdot}10^{6}$).

A specific test rig was designed for the measurement of the steady aerodynamic forces, the vortex-induced vibrations, and the

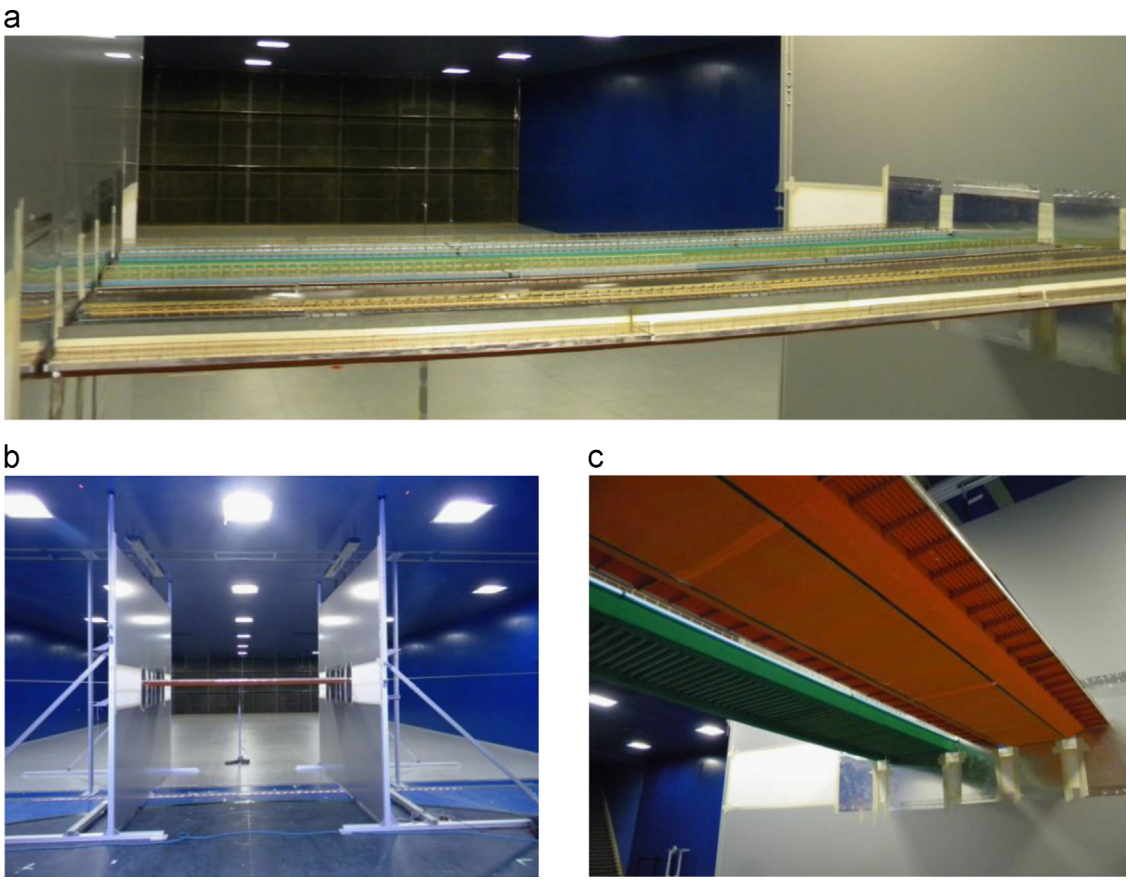

Fig. 4. Experimental test rig: (a) the two sectional models, (b) overall view of the rig; bottom view of the two sectional models.

aeroelastic stability, adopting a bi-dimensional approach. To this end, the test rig consists of two side walls that bound the two sectional models (Fig. 4b). The models are then supported by means of transverse tensioned cables and vertical helical springs that are connected to the walls of the test section.

The ratio between the distance from the mean water level and the depth of the decks is larger than 5, and it was not reproduced in the wind tunnel tests, where this parameter is larger (about five times), since this effect is considered negligible on aerodynamic forces and VIV.

During vortex-induced vibration and aeroelastic tests, the models were suspended and free to vibrate, and their acceleration was measured by means of MEMS accelerometers (sensing range $\pm 2g$, bandwidth 0–250 Hz). Displacements were obtained by post-processing the recorded data. The model eigen-frequencies were tuned selecting the stiffness and the position of the springs, while the structural damping was tuned using two tunable eddy-current dampers. Connections between the suspension system and the models were made using ball-bearings in order to avoid unwanted friction.

During steady aerodynamic force measurements, the new deck was fixed rigidly, while each side of the existing deck was connected to a six-component force balance (strain-gauge balance RUAG type 192) through a constraint that allows the rotation about the axis of the deck, in order to change the angle of attack.

All tests were performed in nominal smooth flow conditions (along-wind turbulence intensity $I_u < 2\%$).

3.2. Similarity laws and scaling factors

For vortex-induced vibration and aeroelastic tests the following scale factors were adopted:

1. The length scale parameter $\lambda_L = \frac{L_M}{L_R} = \frac{1}{50}$, where M identify model quantity and R full scale one.
2. The density scale parameter $\lambda_\rho = \frac{\rho_M}{\rho_R} = 1$ (same fluid: air)
3. The reduced velocity parameter $\lambda_{V^*} = \frac{V^*_M}{V^*_R} = 1$. The reduced velocity is defined as $V^* = V/(fB)$, where V is the mean wind velocity, B is the deck chord of the new deck, and f is the vibration frequency.
4. The Scruton number parameter, or mass-damping parameter, $\lambda_{Sc} = \frac{Sc_M}{Sc_R} \leq 1$. For the vertical modes, the Scruton number is defined as $Sc = m(2\pi\zeta)/(\rho B^2)$, where m is the deck mass per unit length and ζ is the damping ratio coefficient; for the torsional modes, $Sc = J(2\pi\zeta)/(\rho B^4)$, where J is the deck moment of inertia per unit length.

As a consequence of the previous relationships, the velocity scale depends on the frequency scale (which was set between 5 and 6 for the different configurations tested):

$$\frac{V^*_M}{V^*_R} = 1 \quad \Rightarrow \quad \lambda_V = \frac{V_M}{V_R} = \lambda_L \lambda_f \tag{1}$$

The Scruton number similarity is achieved acting both on mass and damping scale factors, λ_ζ and λ_m:

$$\lambda_{Sc} = \frac{Sc_M}{Sc_R} = \frac{\lambda_\zeta \lambda_m}{\lambda_\rho \lambda_L^2} \leq 1 \tag{2}$$

Indeed, the mass and moment of inertia per unit length scale factors that nominally are

$$\lambda_m = \lambda_L^2 \lambda_\rho = \lambda_L^2; \quad \lambda_J = \lambda_L^4 \lambda_\rho = \lambda_L^4 \tag{3}$$

can be taken smaller, in a conservative way for aeroelastic stability, while allowing for more flexibility in the investigation of a wide range of Sc values, tuning only the damping of the aeroelastic model. In other words, if the model is designed lighter than it should be ($\lambda_m < \lambda_L^2$), its Sc number will be lower than it should $\lambda_{Sc} < 1$, but this can be adjusted acting on the damping value ($\lambda_\zeta > 1$), which can be tuned more easily. In particular, the sectional models for VIV tests were made with mass scale factors smaller than the nominal one (0.7 times), in order to allow the investigation of a wide range of Scruton numbers, acting on the tunable eddy current dampers.

4. Results

In this section, results about steady aerodynamic forces and vortex-induced vibrations are presented. Free motion tests were also performed to investigate the aeroelastic stability up to the design wind speed (30 m/s), but results are not discussed in this paper because nor instability issues nor other significant events were recorded.

4.1. Steady aerodynamic coefficients

During the different refurbishment stages, the existing deck was expected to rotate of $\pm$ 2°, because of an asymmetric dead loading. Therefore, aerodynamic steady forces were measured varying only the rotation of the existing deck, to investigate the aerodynamic interference between the two decks.

For the existing bridge, steady aerodynamic drag force (F_D), lift force (F_L) and pitching moment (M) are provided in terms of steady force and moment coefficients, C_D, C_L, C_M as a function of the angle of attack α, according to following formulation:

$$C_D = \frac{\bar{F}_D}{\bar{q}BL}, \quad C_L = \frac{\bar{F}_L}{\bar{q}BL}, \quad C_M = \frac{\bar{M}}{\bar{q}B^2L}$$

where B and L represent the characteristic lengths adopted to express the loads in non- dimensional forms (respectively the deck chord and the length of the sectional model); q is the dynamic pressure at deck height, and the overbar sign represents the mean operator. Sign conventions are reported in Fig. 5.

The interference effect of the two decks can be assessed from Fig. 6, where the steady coefficients of the existing bridge are reported as a function of α, for three different arrangements of the deck: the stand-alone deck is compared with the case when it is upwind the new one (Configuration 6), or downwind (Configuration 4). The main interference effect occurs when the new deck shelters the existing one: the drag coefficient drops significantly (about -50% at α=0°); the lift coefficient keeps its positive slope with the angle of attack, but globally shifts towards negative values (C_L from $+0.1$ to -0.57 at α=0°); the moment coefficient, in agreement with the lift, shifts towards negative values, keeping its slope (C_M from $+0.014$ to -0.04 at α=0°). When the existing deck is upwind the new one, there are less significant interference effects: the main effect is a reduction in the drag force for negative and neutral angles of attack (about -35%).

These results are consistent with those reported by Liu et al. (2009) for the Hongdao bridge, when a similar ratio between the length of the gap between the two decks and the deck chord, x, is considered (for Ewijk bridge $x = 3.4/37.2 \approx 0.1$, see Fig. 3). Larsen et al. (2000) reported similar results for the drag reduction, when considering the parallel Duarte bridge ($x \approx 0.6$), and eventually a beneficial slope reduction in the lift and moment coefficients was measured. However it is not possible to relate the change in the coefficients only to the x parameter, because many parameters are involved, first of all the shapes of the two decks and the structure of their wakes.

4.2. Vortex-induced vibrations

Before the refurbishment, the existing bridge in stand-alone configuration did not suffer of any significant vortex-induced vibrations at its operational Scruton number (Sc=0.27 for the

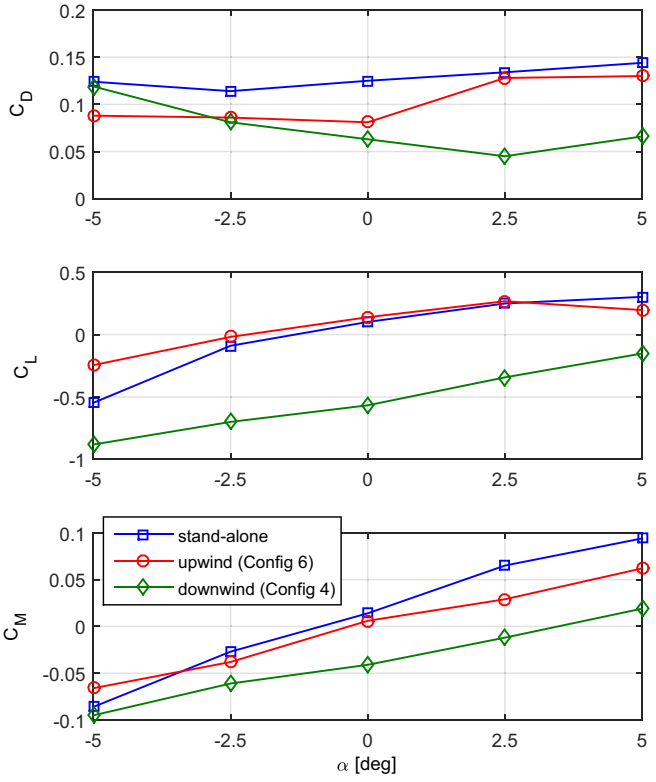

Fig. 6. Existing bridge: comparison of C_D, C_L, C_M as a function of the angle of attack α, for three different configurations.

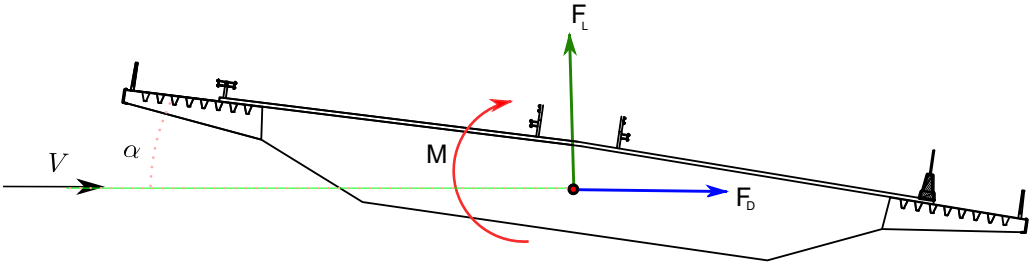

Fig. 5. Sign conventions for drag, lift, and moment.

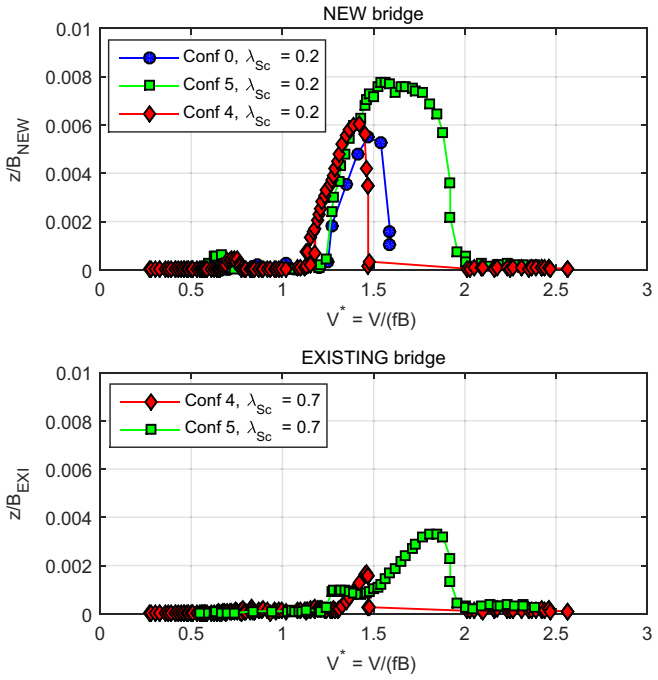

Fig. 7. Non-dimensional vortex induced vertical vibrations for the new and the existing decks as a function of the reduced velocity, for a low *Sc* number, at three different configurations.

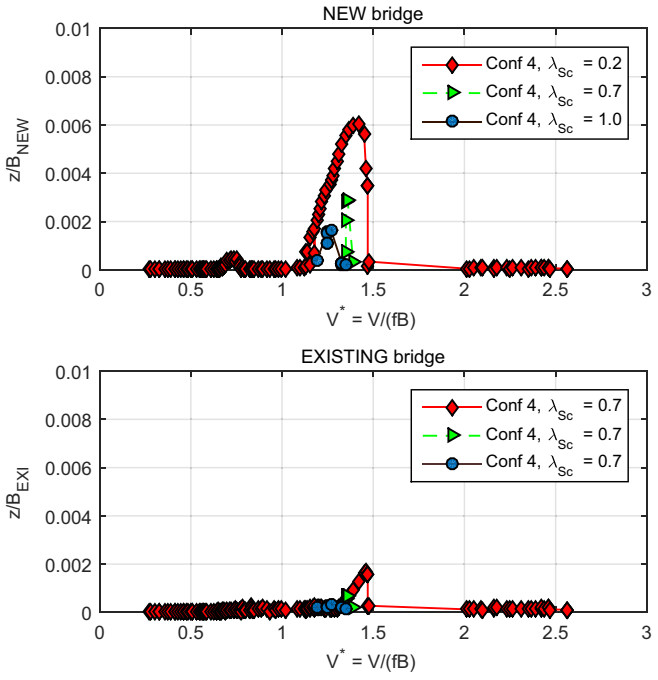

Fig. 8. Non-dimensional vortex induced vertical vibrations for the new and the existing decks as a function of the reduced velocity, for different *Sc* numbers at Configuration 4.

vertical mode, and Sc=0.02 for the torsional one). Therefore, one of the targets of the wind tunnel tests was to investigate if there were any interference effect due to the imminent presence of the new deck, also considering that the two bridges, at in-service condition, have similar eigen-frequencies for the first vertical and torsional modes (respectively, f_v and f_t in Table 2).

Experimental results show that the new bridge, for low Sc values ($\lambda_{Sc} = 0.2$), suffers from vortex shedding excitation for the vertical mode. Fig. 7 reports the VIV response on the decks as a function of the reduced velocity for three configurations: Config 0 is the case of stand-alone new deck (tested for reference); Config 4 is the configuration with the existing deck in the wake of the new one; Config 5 is like Config 4, but with the addition of the optional noise barrier on the new deck. No data are shown for Configuration 6, because in this condition no VIV was recorded.

On one hand, the new bridge response exhibits a classical lock-in range, and the presence of the downstream deck does not influence significantly the VIV response; on the contrary, the lock-in range extension and response amplitude increase if the solid noise barrier at the leading edge of the bridge is present.

On the other hand, the existing bridge seems affected by the VIV response of the upwind deck: this interference is more evident for Configuration 5. It is possible to notice that the range of V^*, where the downstream deck vibrates, coincides with the lock-in region of the upwind deck. Moreover the vibration amplitudes exhibit a nonlinear dependence upon the reduced velocity: for example, in the range $1.5 < V^* < 1.8$ the new deck vibrates at quite steady amplitudes, while the existing deck increases the vibration amplitude approximately linearly with V^* (1 to 3 amplification).

This interference effect is due to the vortexes shed from the upstream deck that forces harmonically the downwind deck. To support this statement, two considerations can be added:

1. if the *Sc* of the new deck is increased ($\lambda_{Sc} = 0.7$ or 1.0) its VIV disappears, and so does the vibration of the existing deck (see Fig. 8).

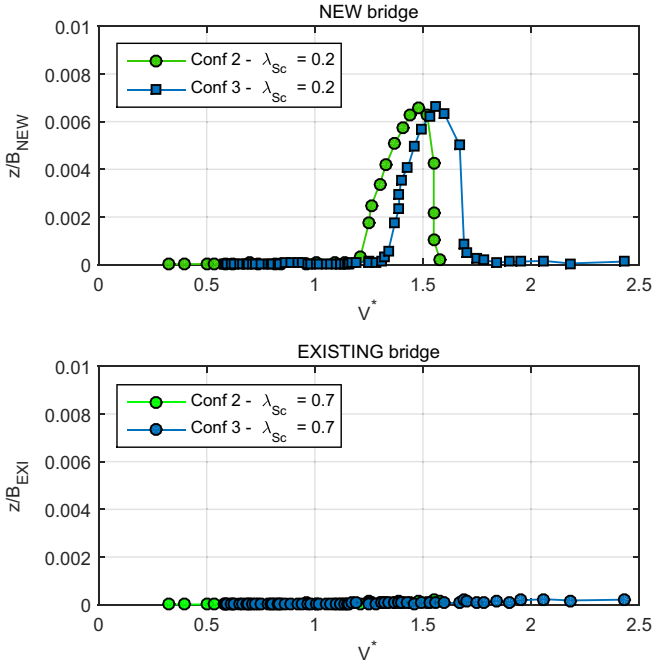

Fig. 9. Non-dimensional vortex induced vertical vibrations for the new and the existing decks as a function of the reduced velocity, for Configurations 2 and 3.

2. if the two bridges have well separated frequencies, as it happens in the refurbishment stages, where the ratio of the vertical frequencies is 1.3 instead of the 0.95 of the in-service configuration, the downstream vibration is not present (see Fig. 9).

This interference can be further analyzed looking at the transfer function between the vertical oscillations of the two decks. In particular, looking at the phase shift $\Delta\phi$ between the displacements of the two decks in the lock-in range, reported in Table 3, it is possible to

Table 3
Phase shift $\Delta\phi$ as a function of the reduced velocity. The negative value indicates that the displacement of the existing (downwind) is in delay with respect to the new bridge.

V^*	$\Delta\phi$ (deg)
1.3	−296
1.4	−250
1.5	−202
1.65	−150
1.8	−120

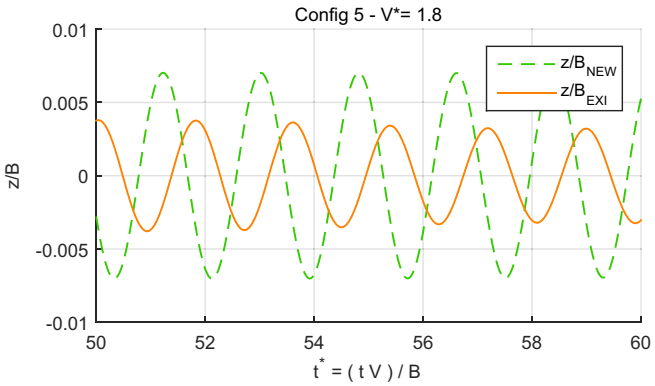

Fig. 10. Non-dimensional vortex induced vertical vibrations for the new and the existing decks as a function of the reduced time, for Configuration 5, at $V^* = 1.8$ (cf. Fig. 7).

notice that it varies almost linearly with the reduced velocity. Fig. 10 shows the time histories of the two vertical responses at $V^* = 1.8$ where the phase shift is about $-120°$.

This phase shift is correlated to the vibration amplitude of the downstream deck, that also increase with the reduced velocity. Therefore, it seems that to force efficiently the downwind deck three conditions should be met:

1. the upwind deck should move to create strong whirling structures able to force the downwind deck
2. the frequencies of the two decks should be close enough in order to force the downwind deck at resonance
3. The combination of

(a) the dimensions and the distance of the two decks
(b) the reduced velocity
(c) the phase between the displacement of the two decks

should synchronize in a way that allows the vortexes shed from the upwind deck to cross the downwind deck at the right time, in order to increase the energy of the downwind deck.

For example, making the hypothesis that the vortex is shed from the wind barriers on the upwind deck and that it travels along the upper surface of the deck when it is moving upwards, the more efficient combination of the aforementioned parameters is reached at $V^* = 1.8$ and $\Delta\phi = -130°$, so that the existing bridge is moving upwards with large velocity when the vortex approaches its leading edge. An animated sketch illustrates this concept (see Supplementary data).

However, this seems a complex behavior and deeper studies should be carried on, since no discussions on this topic can be found in the literature.

5. Conclusions

The aerodynamic interaction of two different adjacent parallel bridges was studied by means of wind tunnel tests on sectional scale models. The large-scale of the models allowed to reproduce geometric details with accuracy, and it is well suited for the measurement of steady aerodynamic forces, and for the study of vortex shedding and vortex-induced vibrations.

The two bridges are close to each other and have similar frequencies. In this condition the aerodynamic interference effect is present both for the steady aerodynamic forces and for the vortex-induced vibrations. In particular the experimental results highlighted that a forcing effect is present on the downwind bridge if the upwind bridge is subjected to VIV when the two decks have similar frequencies. The time shift of the vertical vibration of the two decks varies within the lock-in range of the upwind deck, and when the V^* and the $\Delta\phi$ reach an efficient energy introduction an amplification of the motion of the downwind deck was recorded. For the considered case, no torsional vibrations, nor aeroelastic instabilities were recorded up to the design wind velocity.

As already reported by other researches (e.g. Kimura et al., 2008) it is not possible to generalize the results since they depend on the specific case analyzed, however the experimental results confirm the necessity of tunnel testing to assess the safety of parallel bridges, in order to eventually identify efficient countermeasures to aerodynamic problems.

Appendix A. Supplementary data

Supplementary data associated with this article can be found in the online version.

References

Honda, A., Shiraishi, N., Motoyama, S., 1990. Aerodynamic stability of Kansai international airport access bridge. J. Wind Eng. Ind. Aerodyn. 33, 369–376. http://dx.doi.org/10.1016/0167-6105(90)90052-E.

Irwin, P., Stoyanoff, S., Xie, J., Hunter, M., 2005. Tacoma narrows 50 years later-wind engineering investigations for parallel bridges. Bridge Struct. 1, 3–17. http://dx.doi.org/10.1080/15732480420002745 51.

Kim, S.J., Kim, H.K., Calmer, R., Park, J., Kim, G., Lee, D., 2013. Operational field monitoring of interactive vortex-induced vibrations between two parallel cable-stayed bridges. J. Wind Eng. Ind. Aerodyn. 123, 143–154. http://dx.doi.org/10.1016/j.jweia.2013.10.001.

Kimura, K., Shima, K., Sano, K., Kubo, Y., Kato, K., Ukon, H., 2008. Effects of separation distance on wind-induced response of parallel box girders. J. Wind Eng. Ind. Aerodyn. 96, 954–962. http://dx.doi.org/10.1016/j.jweia.2007.06.021.

Larsen, S.V., Astiz, M.A., Larose, G.L., 2000. Aerodynamic interference between two closely spaced cable supported bridges. In: Fourth International Colloquium on Bluff Body Aerodynamics and Applications, Ruhr-University Bochum, Germany, pp. 33–37.

Liu, Z., Chen, Z., Liu, G., Shao, X., 2009. Experimental study of aerodynamic interference effects on aerostatic coefficients of twin deck bridges. Front. Archit. Civil Eng. China 3, 292–298. http://dx.doi.org/10.1007/s11709-009-0048-8.

Maljaars, J., Vrouwenvelder, T., 2014. Fatigue failure analysis of stay cables with initial defects: Ewijk bridge case study. Struct. Saf. 51, 47–56. http://dx.doi.org/10.1016/j.strusafe.2014.05.007.

Meng, X., Zhu, L., Guo, Z., 2011. Aerodynamic interference effects and mitigation measures on vortex-induced vibrations of two adjacent cable-stayed bridges. Front. Archit. Civil Eng. China 5, 510–517. http://dx.doi.org/10.1007/s11709-011-0129-3.

Okubo, T., Enami, Y., 1972. Results of wind tunnel model tests and field observations of wind effects on the Onomichi bridge. In: Publication of: Precast Concrete UK, Precast Concrete, Public Works Research Institute, Tokyo, pp. 249–260. http://trid.trb.org/view/1972/C/102781.

Seo, J.W., Kim, H.K., Park, J., Kim, K.T., Kim, G.N., 2013. Interference effect on vortex-induced vibration in a parallel twin cable-stayed bridge. J. Wind Eng. Ind. Aerodyn. 116, 7–20. http://dx.doi.org/10.1016/j.jweia.2013.01.014.

Suzuki, Y., Mizuguchi, K., Ueda, T., 1999. Field observation on aerodynamic response of meiko west bridge. In: IABSE Conference (Malmö): Cable-Stayed Bridges: Past, Present and Future, pp. 149–150. http://dx.doi.org/10.5169/seals-62168.

Svensson, H.S., Lovett, T.G., 1990. The twin cable-stayed composite bridge at Baytown, Texas. In: IABSE Symposium (Brussels): Mixed Structures, Including New Materials, pp. 317–322. http://dx.doi.org/10.5169/seals-46499.